Effective electrostatic interactions in colloid-nanoparticle mixtures

Alan R. Denton

Phys. Rev. E **96**, 062610 — Published 18 December 2017

DOI: 10.1103/PhysRevE.96.062610

Effective Electrostatic Interactions in Colloid-Nanoparticle Mixtures

Alan R. Denton*
Department of Physics, North Dakota State University, Fargo, ND, U.S.A. 58108-6050
(Dated: December 4, 2017)

Interparticle interactions and bulk properties of colloidal suspensions can be substantially modified by addition of nanoparticles. Extreme asymmetries in size and charge between colloidal particles and nanoparticles present severe computational challenges to molecular-scale modeling of such complex systems. We present a statistical mechanical theory of effective electrostatic interactions that can greatly ease large-scale modeling of charged colloid-nanoparticle mixtures. By applying a sequential coarse-graining procedure, we show that a multicomponent mixture of charged colloids, nanoparticles, counterions, and coions can be mapped first onto a binary mixture of colloids and nanoparticles and then onto a one-component model of colloids alone. In a linear-response approximation, the one-component model is governed by a single effective pair potential and a one-body volume energy, whose parameters depend nontrivially on nanoparticle size, charge, and concentration. To test the theory, we perform molecular dynamics simulations of the two-component and one-component models and compute structural properties. For moderate electrostatic couplings, colloid-colloid radial distribution functions and static structure factors agree closely between the two models, validating the sequential coarse-graining approach. Nanoparticles of sufficient charge and concentration enhance screening of electrostatic interactions, weakening correlations between charged colloids and destabilizing suspensions, consistent with experiments.

I. INTRODUCTION

Soft materials are typically multicomponent mixtures of components ranging in size and complexity from small molecules to macromolecules, such as polymer coils, compressible microgels, lipid vesicles or dense colloidal particles [1, 2]. Diversity of composition and single-particle properties, and associated tunability of interparticle forces, endow soft matter with unusual mechanical, thermal, optical, and dynamical properties. Rich and tunable materials properties, in turn, enable many practical applications, e.g., in the chemical, petroleum, food, pharmaceutical, and consumer products industries.

With structure and dynamics spanning wide scales of length and time, soft materials pose severe challenges for computational modeling. Especially challenging are materials, such as charge-stabilized colloidal suspensions and polyelectrolyte solutions, in which ion dissociation vastly increases the number of particles and generates long-ranged (Coulomb) electrostatic interparticle forces [3–5]. For such complex systems, coarse-grained models of macroions interacting via effective pair potentials [6, 7] can facilitate selection of system parameters for more explicit models and can guide experiments.

Effective electrostatic interactions in charge-stabilized colloidal suspensions have been modeled by a variety of interrelated liquid-state methods [7], including integral-equation theory [8–16], distribution function theories [17–22], density-functional theory [23–26], and response theory [7, 27–31]. By averaging over microion degrees of freedom, these various approaches all reduce the macroion-microion mixture to a one-component model of pseudo-macroions governed by effective interparticle interactions. When linearized about average microion densities (or average electrostatic potential) and subjected to mean-field approximations for pair correlation functions, these theories are essentially equivalent to linearized Poisson-Boltzmann theory. They thus yield similar results for effective electrostatic pair potentials, differing mainly in the treatment of excluded-volume effects [7, 28, 30].

When pushed beyond the linear-response regime without careful modification, such linearized theories can yield spurious predictions, including thermodynamic phase instabilities [17, 23–25, 32, 33]. Although nonlinear corrections to effective interactions can be systematically derived [31, 34, 35], a more practical approach to addressing nonlinear effects involves charge renormalization. By incorporating nonlinear screening into an effective (renormalized) macroion valence, charge renormalization theories, such as the renormalized Poisson-Boltzmann cell model [36], jellium models [37–42], and one-component models [43–47], significantly extend the range of linearized theories.

In recent years, *mixtures* of charged colloids have attracted considerable interest, as the freedom to tune interparticle interactions by independently varying sizes, charges, and concentrations of different macroion species greatly enhances prospects for controlling thermodynamic phase stability. Particular attention has focused on colloid-nanoparticle mixtures, which are characterized by extreme asym-

* alan.denton@ndsu.edu

metries of size and charge of the different macroion species. Interest has been fueled by the discovery [48] of a new mechanism to stabilize colloidal suspensions against aggregation due to attractive van der Waals interparticle forces, beyond the known mechanisms of steric and charge stabilization.

In a series of experimental studies, Lewis *et al.* [48–52] reported that aggregation of silica microspheres in aqueous suspensions could be inhibited by addition of zirconia or polystyrene nanospheres. These authors postulated that the suspensions were stabilized by the formation of nanoparticle halos around the colloidal particles. Their observations and interpretation have been supported by independent measurements [53–63] confirming that attraction and adsorption of strongly charged nanoparticles onto weakly-charged colloids can result in formation of nanoparticle halos. With increasing concentration, nanoparticles first confer charge stabilization by amplifying the colloid zeta potential, but ultimately destabilize the suspension by screening repulsive electrostatic interactions.

Mixtures of charged colloids have been modeled, e.g., by integral-equation theory [64–73], Poisson-Boltzmann theory [74–78], and computer simulation [79–83]. Motivated by experimental observations, several studies of colloid-nanoparticle mixtures [69, 71, 77, 78, 80] computed effective pair interactions between colloids that are qualitatively consistent with the postulated nanoparticle haloing mechanism. Further studies are needed, however, to chart the multidimensional parameter space.

In this paper, we describe a practical approach to modeling asymmetric mixtures via effective interactions derived from a sequential coarse-graining procedure. As a demonstration, we show that a mixture of charged colloids and nanoparticles can be mapped onto a one-component model of pseudo-macroions governed by an effective Hamiltonian. Physically motivated approximations yield relatively simple, *analytical* expressions for effective interactions, i.e., an effective pair potential and a one-body volume energy, in the one-component model. Inputting the effective pair potential into molecular dynamics simulations, we compute structural properties and establish a criterion for the range of validity of the theory. This hierarchical effective interaction theory provides a systematic and highly efficient means of modeling nanocomposite soft materials.

The remainder of the paper is organized as follows. Section II defines two underlying models of charged colloidal mixtures. Section III develops a theory of effective interactions based on a sequential coarse-graining scheme combined with two practical approximations. Simulation methods used to compute structural properties are outlined in Sec. IV. Section V presents numerical results for radial distribution functions and static structure factors of charged colloid-nanoparticle mixtures over ranges of system parameters, including experimentally relevant parameters. The results validate the theory for systems with moderate electrostatic coupling and establish limits of accuracy of linear-response and mean-field approximations. Section VI concludes with a summary and suggestions for future work.

II. MODELS

A. Primitive Model of Charged Colloids

The system of interest is a mixture of macroions and microions dispersed in a solvent of volume V at temperature T. For simplicity, we consider here a bidisperse mixture of colloids and nanoparticles, although the theory is easily generalized to polydisperse macroion mixtures. The N_c colloids and N_n nanoparticles are modeled as charged hard spheres of respective radii a_c and a_n and valences Z_c and Z_n. The microions comprise N_- coions and N_+ counterions, some dissociated from the macroion surfaces and some originating from added salt, all of equal valence z (symmetric electrolyte). To connect with experiments, the colloidal charge may be viewed as arising either entirely from dissociation of counterions or, at least in part, from surface adsorption of nanoparticles. The average number densities of macroions, microions, and salt ion pairs are denoted by $n_c = N_c/V$, $n_n = N_n/V$, $n_\pm = N_\pm/V$, and n_s, respectively. Under the convention that positive Z_c and Z_n implies negatively charged macroions, global electroneutrality dictates

$$Z_c N_c + Z_n N_n = z(N_+ - N_-) \ . \tag{1}$$

Within the primitive model, the solvent is idealized as a uniform dielectric medium, characterized by a dielectric constant ϵ (Fig. 1). We neglect van der Waals interactions and dielectric polarization effects [84], as any induced polarization charges should hardly influence the structure of the like-charged, weakly-coupled mixtures investigated here. The Hamiltonian of the primitive model includes the kinetic energy and the potential interaction energy of all particles, expressible as a sum over particle pairs of hard-core and Coulomb pair potentials.

B. Coarse-Grained Two-Component Model

Previously, we developed a theory of effective electrostatic interactions in monodisperse suspensions of charged colloids [28–31]. By tracing over the

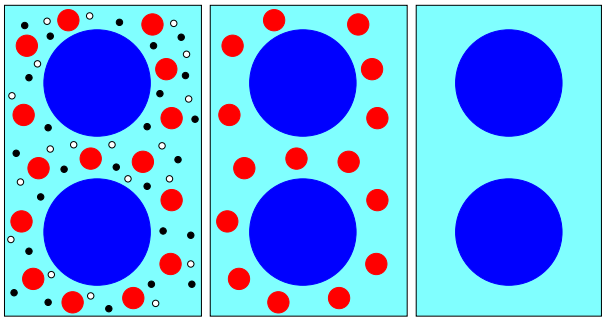

FIG. 1. Left: primitive model of a mixture of charged colloids (blue) and nanoparticles (red) in an implicit solvent with explicit microions (black and white). Middle: coarse-grained two-component model with implicit microions. Right: coarse-grained one-component model with implicit microions *and* nanoparticles.

microion degrees of freedom in the partition function, this theory reduces the macroion-microion mixture to a model comprising only pseudo-macroions, governed by an effective Hamiltonian that comprises effective interactions between macroions and a one-body volume energy, dependent on the average density of the system. Under the assumption that the microion densities respond linearly to the electrostatic potential of the macroions, the pseudo-macroions interact via an effective electrostatic pair potential. (Nonlinear response entails effective many-body interactions [31].) In a random-phase approximation for the microion response functions, which neglects all but long-range correlations between microions, the effective electrostatic pair potential takes a simple repulsive Yukawa (screened-Coulomb) form:

$$v_{\rm eff}(r) = Z_c^2 \lambda_B \left(\frac{e^{\kappa a_c}}{1+\kappa a_c} \right)^2 \frac{e^{-\kappa r}}{r} \ , \quad r \geq 2a_c \ , \quad (2)$$

where r is the center-center distance between two colloids, $\lambda_B = e^2/(\epsilon k_B T)$ is the Bjerrum length, k_B is the Boltzmann constant, and

$$\kappa = \sqrt{\frac{4\pi z^2 \lambda_B (|Z_c| n_c + 2 n_s)}{1-\phi_c}} \quad (3)$$

is the Debye screening constant, which includes a correction for the volume fraction, $\phi_c = (4\pi/3) n_c a_c^3$, excluded to the microions by the colloid hard cores. In Eq. (2) and throughout the paper energies are expressed in thermal ($k_B T$) units.

Recently, Chung and Denton [85] generalized this coarse-graining approach to polydisperse colloidal suspensions. The theory again proceeds by averaging over microion degrees of freedom to map the multicomponent macroion-microion mixture onto a model of only pseudo-macroions governed by an effective Hamiltonian. In linear-response and random-phase approximations, the pseudo-macroions interact via effective pair potentials that combine hard-core and repulsive Yukawa pair potentials. In the case of a bidisperse suspension, one macroion species labelled colloids and the other nanoparticles, the Hamiltonian can be expressed as

$$H = E_0 + H_c + H_n + H_{cn} \ , \quad (4)$$

where E_0 is the volume energy, H_c and H_n are the pseudo-colloid and pseudo-nanoparticle Hamiltonians, respectively, and H_{cn} is the effective colloid-nanoparticle interaction energy. The effective electrostatic pair potentials, of which H_c, H_n, and H_{cn} are summations over particle pairs, take the forms

$$v_{cc}(r) = Z_c^2 \lambda_B \left(\frac{e^{\kappa a_c}}{1+\kappa a_c} \right)^2 \frac{e^{-\kappa r}}{r} \ , \quad r \geq 2a_c \ , \quad (5)$$

$$v_{nn}(r) = Z_n^2 \lambda_B \left(\frac{e^{\kappa a_n}}{1+\kappa a_n} \right)^2 \frac{e^{-\kappa r}}{r} \ , \quad r \geq 2a_n \ , \quad (6)$$

$$v_{cn}(r) = \frac{Z_c Z_n \lambda_B e^{\kappa a_{cn}}}{(1+\kappa a_c)(1+\kappa a_n)} \frac{e^{-\kappa r}}{r} \ , \quad r \geq a_{cn} \ , \quad (7)$$

where $a_{cn} \equiv a_c + a_n$ is the sum of the particle radii and the Debye screening constant generalizes to

$$\kappa = \sqrt{\frac{4\pi z^2 \lambda_B (|Z_c| n_c + |Z_n| n_n + 2 n_s)}{1-\phi}} \quad (8)$$

with $\phi = (4\pi/3)(n_c a_c^3 + n_n a_n^3)$ being the fraction of volume excluded to the microions by both colloid and nanoparticle hard cores. Microions of nonzero size can be easily accommodated by increasing the effective radii of the macroions by the microion radius and adjusting the excluded volume accordingly.

The volume energy of the two-component model takes the explicit form

$$E_0 = F_p - \frac{\lambda_B}{2} \left(\frac{Z_c^2 N_c}{a_c + \kappa^{-1}} + \frac{Z_n^2 N_n}{a_n + \kappa^{-1}} \right) - \frac{1}{2} \frac{(N_+ - N_-)^2}{N_+ + N_-} \ , \quad (9)$$

where on the right side the first term is the free energy of an unperturbed microion plasma, the second term is the self energy of the macroions embedded in the microion plasma, and the third term is the Donnan energy [30, 31, 85]. Treating the microions as a weakly-coupled plasma, excluded from the macroion hard cores,

$$F_p = N_+ \left[\ln \left(\frac{n_+ \Lambda^3}{1-\phi} \right) - 1 \right] + N_- \left[\ln \left(\frac{n_- \Lambda^3}{1-\phi} \right) - 1 \right] , \quad (10)$$

with Λ being the microion thermal wavelength.

Equations (5)-(10) describe a model of a binary mixture of particles governed by an effective Hamiltonian comprising repulsive hard-core-Yukawa effective pair potentials and a density-dependent one-body volume energy. It is important to recall that this model is derived from a coarse-graining procedure applied to the primitive model of a mixture of macroions and explicit microions interacting via Coulomb pair potentials. In the two-component model, the microions are represented only implicitly in the effective interparticle interactions.

III. THEORY

A. Sequential Coarse-Graining Procedure and Reduction to One-Component Model

Starting now from the two-component model with Yukawa effective pair potentials, we next perform a second coarse-graining step, tracing further over the nanoparticle degrees of freedom in the partition function

$$\langle\langle \exp(-H)\rangle_n\rangle_c = \langle \exp(-H_{\rm eff})\rangle_c \ , \qquad (11)$$

where $\langle\ \rangle_c$ and $\langle\ \rangle_n$ denote traces over colloid and nanoparticle degrees of freedom, respectively. In this way, we map the colloid-nanoparticle mixture onto a one-component model of only pseudo-colloids, governed by an effective Hamiltonian

$$H_{\rm eff} = E_0 + H_c + F_n \qquad (12)$$

in which

$$F_n = -\ln\langle \exp(-H_n - H_{cn})\rangle_n \ . \qquad (13)$$

In the canonical ensemble, F_n is interpreted as the Helmholtz free energy of the nanoparticles in the presence of fixed colloids. If the theory were alternatively formulated in the semigrand ensemble, with a reservoir maintaining salt and nanoparticle chemical potentials [33, 47], then F_n would represent the semigrand potential.

Regarding the colloid-nanoparticle effective interaction [Eq. (7)] as an external potential for the nanoparticles, perturbation theory provides an exact expression for the nanoparticle free energy [86]:

$$F_n = F_{n0} + \int_0^1 d\lambda\ \langle H_{cn}\rangle_\lambda \ . \qquad (14)$$

The first term on the right side is the free energy of a reference suspension of nanoparticles, unperturbed by colloid-nanoparticle interactions, but restricted to the free volume, $V' = V/(1-\phi')$, unoccupied by the colloid hard cores, $\phi' = (4\pi/3)n_c a_{cn}^3$ being the volume fraction excluded by the colloids to the nanoparticles. In the second term, $\langle H_{cn}\rangle_\lambda$ denotes an ensemble average of the colloid-nanoparticle interaction energy in a system in which the colloids are charged to a fraction λ of their full charge. Further progress is facilitated by expressing $\langle H_{cn}\rangle_\lambda$ in terms of the colloid-nanoparticle effective pair potential and the local densities of colloids and nanoparticles:

$$\begin{aligned}\langle H_{cn}\rangle_\lambda &= \int_{V'} d\mathbf{r} \int_{V'} d\mathbf{r}'\, v_{cn}(|\mathbf{r}-\mathbf{r}'|) n_c(\mathbf{r})\, \langle n_n(\mathbf{r}')\rangle_\lambda \\ &= \frac{1}{V'}\sum_{\mathbf{k}} \hat{v}_{cn}(k)\hat{n}_c(\mathbf{k})\, \langle \hat{n}_n(-\mathbf{k})\rangle_\lambda \ , \end{aligned} \qquad (15)$$

where $\hat{v}_{cn}(k)$, $\hat{n}_c(\mathbf{k})$, and $\hat{n}_n(\mathbf{k})$ are the respective Fourier transforms.

B. Linear-Response Approximation

While the coarse-graining procedure summarized by Eqs. (11)-(15) is exact, deriving practical expressions for effective interactions requires approximations. Just as the two-component model with Yukawa effective pair potentials emerges from the primitive model upon assuming that the microions respond linearly to the macroion-microion potential, similarly we assume that the nanoparticles respond linearly to the colloid-nanoparticle effective potential. The nanoparticle density can be separated, according to $n_n(\mathbf{r}) = n_{n0}(\mathbf{r}) + n_{n1}(\mathbf{r})$, into a reference term $n_{n0}(\mathbf{r})$ (unperturbed density in the absence of electrostatic response) and a perturbation term $n_{n1}(\mathbf{r})$ (response to colloids). The reference density will be fixed below by requiring that the nanoparticles are excluded from the colloid hard cores.

In the linear-response approximation, $n_{n1}(\mathbf{r})$ depends linearly on the "external" potential $\phi_{cn}(\mathbf{r})$ of the colloids acting on the nanoparticles:

$$n_{n1}(\mathbf{r}) = \int_{V'} d\mathbf{r}'\, \chi_n(|\mathbf{r}-\mathbf{r}'|)\phi_{cn}(\mathbf{r}') \ , \qquad (16)$$

where

$$\phi_{cn}(\mathbf{r}) = \int_{V'} d\mathbf{r}'\, v_{cn}(|\mathbf{r}-\mathbf{r}'|) n_c(\mathbf{r}') \ . \qquad (17)$$

The nanoparticle linear-response function, formally defined as [86]

$$\chi_n(|\mathbf{r}-\mathbf{r}'|) = \frac{\delta n_n(\mathbf{r})}{\delta\phi_{cn}(\mathbf{r}')} \ , \qquad (18)$$

relates a change in nanoparticle density at position $\mathbf{r}$ to a change in external potential at position $\mathbf{r}'$

and is related to the nanoparticle-nanoparticle pair correlation function $h_{nn}(r)$ via

$$\chi_n(|\mathbf{r}-\mathbf{r}'|) = -\tilde{n}_n[\delta(|\mathbf{r}-\mathbf{r}'|)+\tilde{n}_n h_{nn}(|\mathbf{r}-\mathbf{r}'|)] \ , \quad (19)$$

with $\tilde{n}_n \equiv n_n/(1-\phi')$ being the nanoparticle number density in the free volume V'. Fourier transforming Eq. (16) yields the linear-response approximation for the nanoparticle density profile in k-space:

$$\hat{n}_{n1}(k) = \hat{\chi}_n(k)\hat{v}_{cn}(k)\hat{n}_c(k) \ , \quad (20)$$

where the Fourier transform of the nanoparticle linear-response function,

$$\hat{\chi}_n(k) = -\tilde{n}_n[1+\tilde{n}_n\hat{h}_{nn}(k)] \ , \quad (21)$$

is proportional to the nanoparticle-nanoparticle static structure factor. Substituting Eq. (16) or (20) into Eq. (15) and combining Eqs. (11)-(15), allows $H_{\rm eff}$ to be recast as a pairwise sum of an effective colloid-colloid pair potential, an explicit expression for which is derived in Sec. III E.

C. Random-Phase Approximation

Further progress in mapping the two-component model onto a one-component model requires approximating the nanoparticle linear-response function, exploiting its relation to the nanoparticle-nanoparticle direct correlation function $\hat{c}_{nn}(k)$:

$$\hat{\chi}_n(k) = -\frac{\tilde{n}_n}{1-\tilde{n}_n\hat{c}_{nn}(k)} \ . \quad (22)$$

In the mean-field random-phase approximation, which neglects all but long-range correlations between nanoparticles, $\hat{c}_{nn}(k) \simeq -\hat{v}_{nn}(k)$, and thus

$$\hat{\chi}_n(k) = -\frac{\tilde{n}_n}{1+\tilde{n}_n\hat{v}_{nn}(k)} \ . \quad (23)$$

Assuming that the nanoparticles respond as point particles, which is reasonable for charged particles whose hard cores interact only weakly,

$$\hat{v}_{nn}(k) \simeq \frac{4\pi c_n}{k^2+\kappa^2} \quad (24)$$

with

$$c_n \equiv Z_n^2\lambda_B\left(\frac{e^{\kappa a_n}}{1+\kappa a_n}\right)^2 \ , \quad (25)$$

which follows from Eq. (6) extended into the range $r < 2a_n$. Combining Eqs. (23) and (24), we have

$$\hat{\chi}_n(k) = -\tilde{n}_n\,\frac{k^2+\kappa^2}{k^2+\kappa^2+\kappa_n^2} \ , \quad (26)$$

where

$$\kappa_n \equiv \sqrt{4\pi c_n\tilde{n}_n} \quad (27)$$

plays the role of an effective nanoparticle-induced screening constant. The corresponding random-phase approximation for the nanoparticle-nanoparticle pair correlation function is

$$\hat{h}_{nn}(k) = -\frac{1}{\tilde{n}_n}\left[1+\frac{\hat{\chi}(k)}{\tilde{n}_n}\right] = -\frac{4\pi c_n}{k^2+q^2} \ , \quad (28)$$

or in real space,

$$h_{nn}(r) = -c_n\frac{e^{-qr}}{r} \ , \quad (29)$$

where

$$q \equiv \sqrt{\kappa^2+\kappa_n^2} \quad (30)$$

is interpreted as an effective *nanoparticle-enhanced* screening constant. From Eqs. (25) and (30), it can be seen that the nanoparticles contribute to screening the electrostatic interactions between the colloids as would point charges of effective valence

$$Z_{n,\rm eff} = \frac{e^{\kappa a_n}}{1+\kappa a_n}Z_n \ , \quad (31)$$

consistent with an assumption made in a theory of nanoparticle adsorption by dos Santos *et al.* [87]. We are now in position to derive explicit expressions for the nanoparticle density profile and the effective colloid-colloid pair potential.

D. Nanoparticle Density Profile

Having approximated the nanoparticle linear-response function, we can now calculate the nanoparticle density profile around a single colloid, $n_n(r)$, from Eqs. (16), (19), and (29). Since impenetrability of the colloid and nanoparticle cores is enforced by the hard-core component of the effective colloid-nanoparticle pair potential, the form of the electrostatic component for overlapping cores is arbitrary. We are free, therefore, to specify the form of $v_{cn}(r)$ for $r < a_{cn}$, which we do to ensure exclusion of the nanoparticles from the colloid hard cores, i.e., $n_n(r) = 0$ for $r < a_{cn}$. For simplicity, we choose $v_{cn}(r)$ to be a constant for overlapping cores:

$$v_{cn}(r) = \alpha\frac{Z_cZ_n\lambda_B}{(1+\kappa a_c)(1+\kappa a_n)a_{cn}} \ , \quad r < a_{cn} \ , \quad (32)$$

where α is a constant yet to be determined.

Substituting Eqs. (19), (29), and (32) into Eq. (16), we find

$$n_{n1}(r) = A\tilde{n}_n e^{\kappa_0}\left[-f(r)+\frac{\kappa_n^2}{2}\,I_1(r)\right] \ , \quad (33)$$

where

$$A \equiv \frac{Z_c Z_n \lambda_B}{(1+\kappa a_c)(1+\kappa a_n)} \ , \tag{34}$$

$$f(r) = \begin{cases} \dfrac{e^{-\kappa r}}{r} \ , & r \geq a_{cn} \\ \alpha \ \dfrac{e^{-\kappa_0}}{a_{cn}} \ , & r < a_{cn} \ , \end{cases} \tag{35}$$

and

$$I_1(r) = \int_{-1}^{1} d\mu \int_0^\infty dr' \, r' e^{-qr'} f(|\mathbf{r}-\mathbf{r}'|) \ , \tag{36}$$

with $\mu \equiv \cos\theta$, θ being the angle between the vectors $\mathbf{r}$ and $\mathbf{r}'$. As shown in the Appendix, the integral $I_1(r)$ can be evaluated analytically, with the result

$$I_1(r) = \begin{cases} 2\dfrac{e^{-\kappa_0-q_0}}{\kappa+q}\dfrac{\sinh(qr)}{qr} + \alpha\dfrac{e^{-\kappa_0}}{a_{cn}}\dfrac{2}{q^2}\left[1-(1+q_0)e^{-q_0}\dfrac{\sinh(qr)}{qr}\right] \ , & r < a_{cn} \ , \\ \dfrac{2}{\kappa_n^2 r}(e^{-\kappa r}-e^{-qr}) - \left(\dfrac{e^{q_0-\kappa_0}}{q-\kappa} + \dfrac{e^{-\kappa_0-q_0}}{\kappa+q} - \dfrac{2q}{\kappa_n^2}\right)\dfrac{e^{-qr}}{qr} & \\ +\alpha\dfrac{e^{-\kappa_0}}{a_{cn}}\left[(q_0-1)e^{q_0}+(1+q_0)e^{-q_0}\right]\dfrac{e^{-qr}}{q^3 r} \ , & r > a_{cn} \ . \end{cases} \tag{37}$$

where $\kappa_0 \equiv \kappa a_{cn}$ and $q_0 \equiv q a_{cn}$. Now substituting Eq. (37) into Eq. (33) and rearranging, we find

$$n_{n1}(r) = -A\tilde{n}_n \begin{cases} \dfrac{\alpha}{a_{cn}}\dfrac{\kappa_0^2}{q_0^2} + \left(\dfrac{\alpha+\kappa_0}{q_0} - \alpha\dfrac{\kappa_0^2}{q_0^3} + \alpha - 1 - \alpha\dfrac{\kappa_0^2}{q_0^2}\right)e^{-q_0}\dfrac{\sinh(qr)}{r} \ , & r < a_{cn} \\ \left[\left(\dfrac{\alpha+\kappa_0}{q_0} - \dfrac{\alpha\kappa_0^2}{q_0^3}\right)\sinh q_0 - \left(\alpha - 1 - \dfrac{\alpha\kappa_0^2}{q_0^2}\right)\cosh q_0\right]\dfrac{e^{-qr}}{r} \ , & r \geq a_{cn} \ . \end{cases} \tag{38}$$

To ensure that nanoparticles are excluded from the colloid hard cores, the constant α and function $n_{n0}(r)$ now must be chosen such that

$$\frac{\alpha+\kappa_0}{q_0} - \alpha\frac{\kappa_0^2}{q_0^3} + \alpha - 1 - \alpha\frac{\kappa_0^2}{q_0^2} = 0 \ , \tag{39}$$

that is,

$$\alpha = \frac{q_0}{1+q_0} \ \frac{1}{1+\kappa_0/q_0} \ , \tag{40}$$

and

$$n_{n0}(r) = \frac{A\tilde{n}_n}{a_{cn}} \ \frac{\kappa_0^2}{(1+q_0)(\kappa_0+q_0)} \ , \quad r < a_{cn} \ . \tag{41}$$

The form of $n_{n0}(r)$ outside the hard core is determined by requiring that the volume integral of the nanoparticle density profile around a colloid equals the average number of nanoparticles per colloid:

$$4\pi \int_{a_{cn}}^\infty dr \, r^2 n_n(r) = n_n/n_c \ , \tag{42}$$

which implies

$$n_{n0}(r) = \frac{1}{V}\left(\frac{n_n}{n_c} + 4\pi A\tilde{n}_n \frac{1+\kappa_0}{q^2}\right), \quad r \geq a_{cn} \ . \tag{43}$$

Substituting α from Eq. (40) into Eq. (38) yields

$$n_{n1}(r) = -\frac{A\tilde{n}_n}{(1+q_0)} \begin{cases} \dfrac{\kappa_0^2}{a_{cn}(\kappa_0+q_0)}, & r < a_{cn} \\ (1+\kappa_0)e^{q_0}\dfrac{e^{-qr}}{r}, & r \geq a_{cn} \ . \end{cases} \tag{44}$$

The average nanoparticle density profile centered on any given colloidal particle in a bulk suspension – ensemble averaged over configurations – is given by

$$n_n(r) = n_n^{(1)}(r) + 2\pi n_c \int_0^\infty dR \, R^2 g_{cc}(R) \times \int_{-1}^{1} d\mu \, n_n^{(1)}(|\mathbf{r}-\mathbf{R}|) \ , \tag{45}$$

where $n_n^{(1)}(r) = n_{n0}(r) + n_{n1}(r)$ is the radial density profile around a single colloidal particle [Eqs. (43) and (44)], $g_{cc}(R)$ is the colloid-colloid radial distribution function (see Sec. IV), and $\mu \equiv \cos\theta$, with θ being the angle between position vectors $\mathbf{r}$ and $\mathbf{R}$.

E. Effective Colloid-Colloid Pair Potential

Upon substituting Eq. (16) into Eq. (15), the effective Hamiltonian of the one-component model

[Eq. (12)] can be expressed, in the linear-response approximation, as a sum of effective pair potentials and a one-body volume energy. The effective pair potential between a pair of pseudo-colloids with center-to-center separation r takes the form

$$v_{cc}^{\rm eff}(r) = v_{cc}(r) + v_{cc}^{\rm ind}(r) \ , \quad r \geq 2a_{cn} \ , \qquad (46)$$

where $v_{cc}(r)$ is the bare Yukawa pair potential [Eq. (5)] and

$$v_{cc}^{\rm ind}(r) = \int d\mathbf{r}' \, n_{n1}(r') v_{cn}(|\mathbf{r}-\mathbf{r}'|) \qquad (47)$$

is the *nanoparticle-induced* pair potential with Fourier transform

$$\hat{v}_{cc}^{\rm ind}(k) = \hat{\chi}_n(k) \left[\hat{v}_{cn}(k)\right]^2 = \hat{n}_{n1}(k)\hat{v}_{cn}(k) \ . \qquad (48)$$

It is worth noting that the same general form of Eq. (46) results from integral-equation theory through a formal "contraction of the description" of liquid mixtures, based on the assumption that the one-component model has the same bridge function as the mixture [88, 89]. Furthermore, the mean-spherical approximation (MSA) closure of the Ornstein-Zernike integral equations yields a nanoparticle-induced potential formally similar to Eq. (48). In general, different closures amount to different approximations for nanoparticle correlations. Previous applications of effective-interaction theories – consistently accounting for charge renormalization – have proven the MSA closure to be accurate in predicting thermodynamic and structural properties of charge-stabilized colloidal suspensions [42–47]. The Ornstein-Zernike equations, with the hypernetted-chain (HNC) closure approximation, also can be numerically solved for an explicit mixture of ions interacting via Coulomb pair potentials in the primitive model [90–92]. This more explicit, but computationally intensive, approach should be more accurate in cases of strongly correlated nanoparticles. The resulting potential of mean force between colloids could be used to further assess the range of validity of our effective pair potential with renormalized valences.

An explicit expression for the effective colloid-colloid pair potential follows from substituting Eqs. (7) and (44) into Eq. (47):

$$v_{cc}^{\rm ind}(r) = BI_2(r) + CI_3(r) \ , \qquad (49)$$

with

$$I_2(r) \equiv \int_{-1}^{1} d\mu \int_0^{a_{cn}} dr' \, r'^2 f(|\mathbf{r}-\mathbf{r}'|) \ , \qquad (50)$$

$$I_3(r) \equiv \int_{-1}^{1} d\mu \int_{a_{cn}}^{\infty} dr' \, r' e^{-qr'} f(|\mathbf{r}-\mathbf{r}'|) \ , \qquad (51)$$

and

$$B \equiv C \ \frac{\kappa_0^2 \ e^{-q_0}}{a_{cn}(1+\kappa_0)(\kappa_0+q_0)} \ , \qquad (52)$$

$$C \equiv -2\pi A^2 \tilde{n}_n \ e^{\kappa_0+q_0} \ \frac{1+\kappa_0}{1+q_0} \ . \qquad (53)$$

As shown in the Appendix, for $r \geq 2a_{cn}$, the integrals in Eqs. (50) and (51) evaluate explicitly to

$$I_2(r) = \frac{1}{\kappa^3}[(1+\kappa_0)e^{-\kappa_0} - (1-\kappa_0)e^{\kappa_0}] \ \frac{e^{-\kappa r}}{r} \qquad (54)$$

and

$$I_3(r) = -\frac{2}{\kappa_n^2} e^{q_0-\kappa_0} \ \frac{1+\kappa_0}{1+q_0} \ \frac{e^{-qr}}{r} - \left(\frac{e^{\kappa_0-q_0}}{\kappa-q} + \frac{e^{-\kappa_0-q_0}}{\kappa+q}\right) \frac{e^{-\kappa r}}{\kappa r} \ . \qquad (55)$$

Now substituting Eqs. (52)-(55) into Eq. (49) yields

$$v_{cc}^{\rm ind}(r) = -Z_c^2 \lambda_B \left(\frac{e^{\kappa a_c}}{1+\kappa a_c}\right)^2 \frac{e^{-\kappa r}}{r} + Z_c^2 \lambda_B \left(\frac{e^{(q_0-\kappa a_n)}}{1+q_0} \frac{1+\kappa_0}{1+\kappa a_c}\right)^2 \frac{e^{-qr}}{r} \ . \qquad (56)$$

Combining Eqs. (5), (46), and (56), we arrive at the important result (valid for $r \geq 2a_{cn}$)

$$v_{cc}^{\rm eff}(r) = Z_c^2 \lambda_B \left(\frac{e^{q_0-\kappa a_n}}{1+q_0} \ \frac{1+\kappa_0}{1+\kappa a_c}\right)^2 \frac{e^{-qr}}{r} \ . \qquad (57)$$

Remarkably, the effective pair potential in the one-component model still has the simple Yukawa form, but with modified amplitude and screening constant, which depend nontrivially on the nanoparticle properties (radius, valence, and concentration). Note that, in the limits $Z_n \to 0$ or $n_n \to 0$, as the nanoparticle influence vanishes, $q \to \kappa$ and $v_{cc}^{\rm eff}(r)$ reduces to Eq. (5). Interestingly, the effective pair potential, since it depends only on the square of the colloid-nanoparticle pair potential, is independent of the signs of the two macroion charges. This predicted symmetry, a consequence of the linear-response approximation, is tested in Sec. V.

From Eqs. (12)-(16), the volume energy of the one-component model is given by

$$E = E_0 + F_{n0} + \frac{1}{2} N_c v_{cc}^{\rm ind}(0) \ , \qquad (58)$$

where again E_0 is the volume energy of the *bare* colloid-nanoparticle mixture [Eq. (9)] (before tracing over the nanoparticle degrees of freedom) and

$$F_{n0} = N_n \left[\ln(\tilde{n}_n \Lambda_n^3) - 1\right] \qquad (59)$$

is the ideal-gas free energy of the nanoparticles in the free volume, Λ_n being the thermal wavelength of the nanoparticles. Setting $r = 0$ in Eqs. (50) and (51) and substituting into Eq. (49), we find

$$v_{cc}^{\rm ind}(0) = \frac{2}{3}Be^{-\kappa_0}\alpha a_{cn}^2 + \frac{2}{\kappa+q}Ce^{-\kappa_0-q_0}$$
$$= -4\pi A^2\tilde{n}_n a_{cn}\frac{1+\kappa_0+\alpha\kappa_0^2/3}{(1+q_0)(\kappa_0+q_0)} \ . \quad (60)$$

Note that, unlike the effective pair potential, the volume energy does depend on the signs of the macroion charges through the dependence of E_0 on the numbers of counterions and coions.

Summarizing thus far, the proposed theory of charged colloid-nanoparticle mixtures, based on a coarse-graining scheme that sequentially traces over microion and nanoparticle degrees of freedom, first maps the primitive model onto a two-component model of only colloids and nanoparticles interacting via Yukawa effective pair potentials. The theory then maps the two-component model further onto a one-component model of only colloids interacting via a modified Yukawa effective pair potential [Eq. (57)] with redefined amplitude and screening constant [Eq. (30)], both of which increase with increasing size, charge, and concentration of nanoparticles. The effective Hamiltonian also includes a one-body volume energy, which is relevant for thermodynamic properties. It should be noted that a naive coarse-graining procedure that would treat the nanoparticles on the same footing as the microions, and thus map the primitive model directly onto the one-component model without the intervening two-component model, would yield quite different (and less accurate) effective interactions, reducing to our results only in the limits $a_n \to 0$ and $Z_n \to z$.

In passing, we note that the linear-response theory developed here also could be adapted to planar geometry and applied to predict density profiles of charged nanoparticles adsorbed onto charged walls, as well as induced interactions between parallel walls. Such applications would require extension beyond the random phase approximation to more accurately incorporate correlations between nanoparticles. Predictions could be compared with those of dos Santos *et al.* [87], who modeled adsorption isotherms of charged nanoparticles via a modified Poisson-Boltzmann theory and simulation, and with results of integral-equation theory applied to the structure of charged colloids near charged walls [93, 94]. Next, we discuss computer simulations designed to numerically test the range of accuracy of the effective interaction theory.

IV. COMPUTATIONAL METHODS

To test the effective interaction theory proposed in Sec. III, we performed classical molecular dynamics simulations of both coarse-grained models of charged colloid-nanoparticle mixtures – the two-component model, governed by Eqs. (5)-(8), and the one-component model, governed by Eqs. (30) and (57). The simulations were conducted using the Large-scale Atomic/Molecular Massively Parallel Simulator (LAMMPS) [95, 96] to integrate (via Verlet's method) Newton's equations of motion for fixed numbers of particles in a cubic box of fixed volume, subject to periodic boundary conditions. An average temperature of $T = 293$ K was maintained by a Nosé-Hoover thermostat. Aqueous suspensions were modeled by setting $\lambda_B = 0.714$ nm. The Yukawa pair potentials were truncated at a distance r_c of half the box length, ensuring $r_c > 10/\kappa$ (10 screening lengths) for the system sizes considered. Interactions between macroion hard cores were ignored, since we consider only like-charged (i.e., mutually repulsive) macroions.

All particles were initialized on the sites of a cubic lattice with up to a 16-atom basis, which facilitated variation of the nanoparticle concentration. Following an annealing stage of 10^5 steps, during which the temperature was steadily ramped down from 1000 K to 293 K, and an equilibration stage of 10^5 steps, we computed structural quantities by averaging over particle trajectories for an additional 10^6 time steps. From particle configurations, we computed the partial radial distribution functions,

$$g_{\alpha\beta}(r) = \frac{V}{x_\alpha x_\beta N^2}\sum_{i=1}^{N_\alpha}{\sum_{j=1}^{N_\beta}}' \langle\delta(\mathbf{r}+\mathbf{r}_j-\mathbf{r}_i)\rangle \ , \quad (61)$$

and the partial static structure factors [86],

$$S_{\alpha\beta}(k) = x_\alpha\delta_{\alpha\beta} + \frac{1}{N}\sum_{i=1}^{N_\alpha}{\sum_{j=1}^{N_\beta}}' \left\langle\frac{\sin(kr_{ij})}{kr_{ij}}\right\rangle \ , \quad (62)$$

where $x_\alpha = N_\alpha/N$ is the concentration of species α, $\delta(\mathbf{r})$ is the Dirac delta function, $\delta_{\alpha\beta}$ is the Kronecker delta function, the prime on the sum means self-interactions are excluded, and angular brackets represent a time average. In computing averages, we sampled configurations at intervals of 10^3 time steps. We are especially interested in comparing the colloid-colloid radial distribution function and static structure factor in the two-component model,

$$g_{cc}(r) = \frac{V}{N_c^2}{\sum_{i,j=1}^{N_c}}' \langle\delta(\mathbf{r}+\mathbf{r}_j-\mathbf{r}_i)\rangle \ , \quad (63)$$

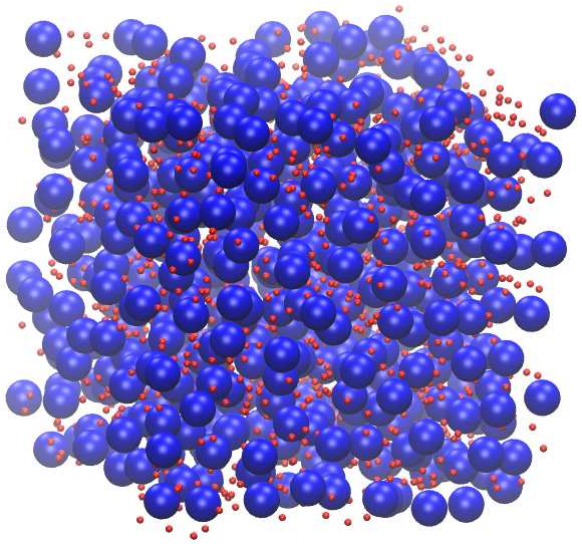

FIG. 2. Snapshot from molecular dynamics simulation of coarse-grained two-component model of a mixture of charged colloids (blue) and charged nanoparticles (red). Microions and solvent are implicit in effective interparticle interactions.

$$S_{cc}(k) = x_c + \frac{1}{N}\sum_{i,j=1}^{N_c}{}' \left\langle \frac{\sin(kr_{ij})}{kr_{ij}} \right\rangle \ , \qquad (64)$$

with their counterparts, $g(r)$ and $S(k)$, in the coarse-grained one-component model, noting that for a direct comparison, $S_{cc}(k)$ must be scaled by the colloid concentration:

$$S(k) = \frac{S_{cc}(k)}{x_c} = 1 + \frac{1}{N_c}\sum_{i,j=1}^{N_c}{}' \left\langle \frac{\sin(kr_{ij})}{kr_{ij}} \right\rangle \ . \qquad (65)$$

V. RESULTS AND DISCUSSION

A. Validation of One-Component Model

Elsewhere we analyzed the influence of charged nanoparticles on the structure and stability of charge-stabilized colloidal suspensions [97]. Here we focus on testing the effective interaction theory developed in Sec. III and assessing the reliability of mapping the two-component model onto the one-component model. To this end, we performed a series of simulations, using the methods described in Sec. IV, and computed structural properties of charged colloid-nanoparticle mixtures. To limit the vast parameter space, we fixed the colloid and nanoparticle numbers at $N_c = 500$ and $N_n = 1500$, the particle radii at $a_c = 50$ nm and $a_n = 5$ nm, considered only salt-free systems ($n_s = 0$) with monovalent microions ($z = 1$), and varied only the macroion valences and volume fractions. Figure 2 shows a snapshot from a typical run.

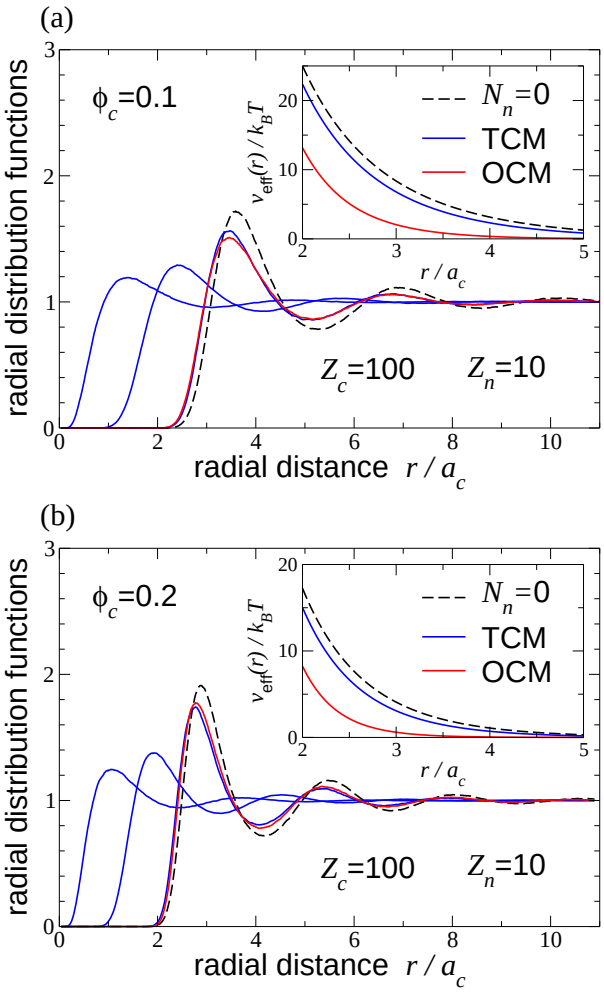

FIG. 3. Radial distribution functions from MD simulations of coarse-grained models of colloid-nanoparticle mixtures. Blue curves are, from right to left by main peak position, $g_{cc}(r)$, $g_{cn}(r)$, and $g_{nn}(r)$ in the two-component model (TCM). Red and dashed black curves are, respectively, $g_{cc}(r)$ in the one-component model (OCM) and the nanoparticle-free suspension ($N_n = 0$). System parameters are colloid number $N_c = 500$, radius $a_c = 50$ nm, and valence $Z_c = 100$; nanoparticle number $N_n = 1500$, radius $a_n = 5$ nm, and valence $Z_n = 10$. Colloid volume fractions are $\phi_c = 0.1$ (a) and 0.2 (b). Beyond main peak, TCM and OCM curves are barely distinguishable. Insets: Effective colloid-colloid pair potentials, $v_{\rm eff}(r)$, in TCM and OCM.

Figures 3-5 show our numerical results for radial distribution functions in both the two-component model (TCM) and one-component model (OCM). For reference, $g_{cc}(r)$ of the nanoparticle-free suspension is also shown. Further quantifying the

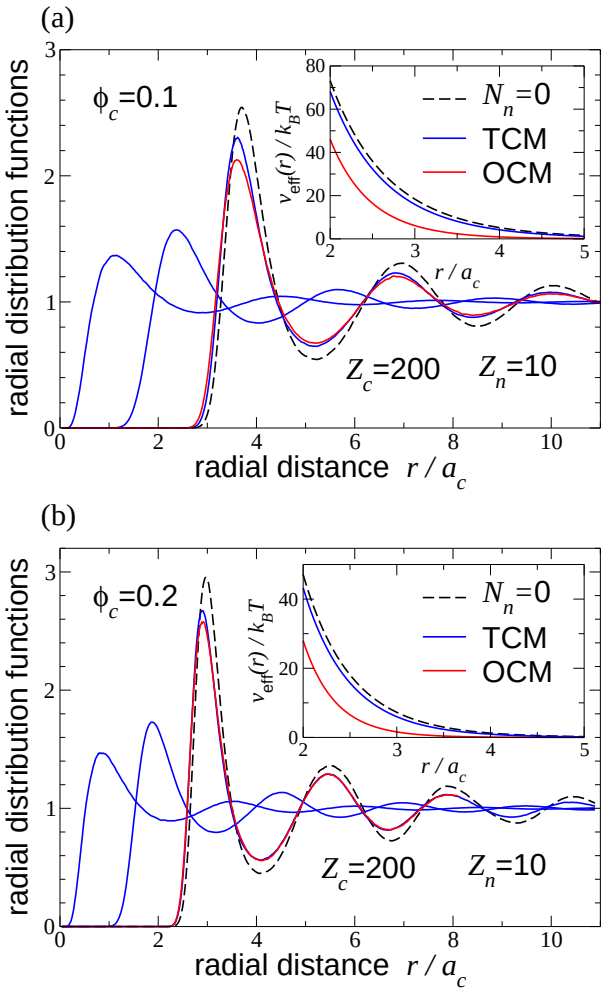

FIG. 4. Same as Fig. 3, but for colloid and nanoparticle valences $Z_c = 200$ and $Z_n = 10$. Beyond main peak, TCM and OCM curves are barely distinguishable.

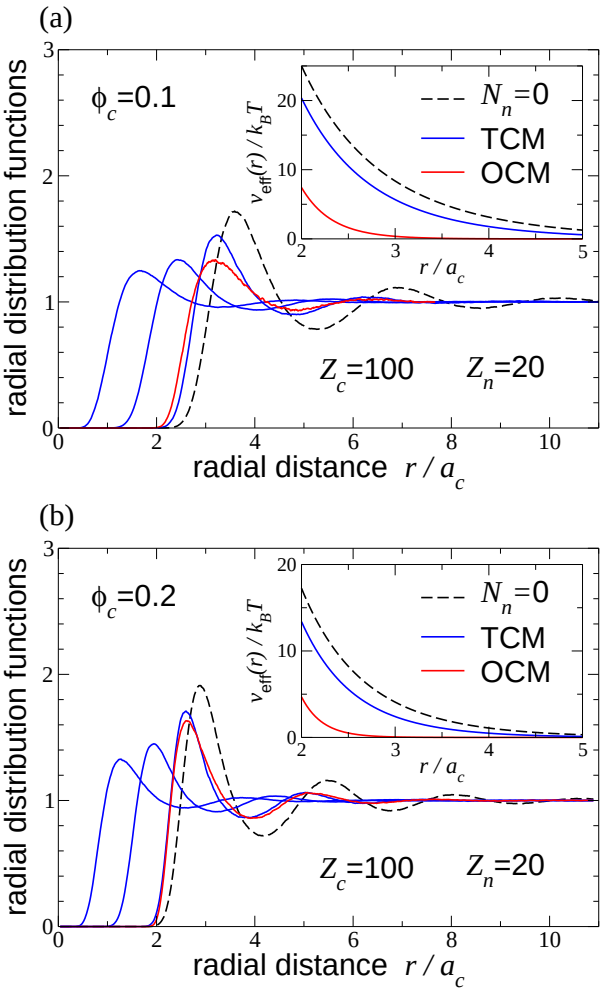

FIG. 5. Same as Fig. 3, but for colloid and nanoparticle valences $Z_c = 100$ and $Z_n = 20$.

structural comparisons, we also computed the complementary colloid-colloid static structure factors (Fig. 6). The close agreement between the TCM and the OCM is quite remarkable, considering the nontrivial nature of the modified screening constant q and amplitude in the effective pair potential.

For all cases considered, adding charged nanoparticles softens the structure of a suspension of charged colloids, as reflected by the lower peak heights of $g_{cc}(r)$ and $S_{cc}(k)$. This weakening of colloid-colloid correlations is accompanied by a decreasing range and amplitude of the effective colloid-colloid pair potential (insets to Figs. 3-5), which results from a larger screening constant κ in the presence of nanoparticles. Enhancement of screening by charged nanoparticles is associated with nanoparticle haloing around colloids, as reflected by significant colloid-nanoparticle correlations and quantified by the prominent main peak of $g_{cn}(r)$ seen in Figs. 3-5. This interpretation is consistent with the integral-equation theory study of Chávez-Páez *et al.* [70], who established two criteria for nanoparticle haloing: (1) the colloidal diameter should exceed three times the mean nearest-neighbor distance between nanoparticles and (2) the nanoparticles should behave as a highly-structured fluid. Both of these criteria are indeed met in our systems. Moreover, colloid-nanoparticle correlations grow stronger with increasing volume fraction, i.e., decreasing mean nanoparticle spacing, as seen by comparing panels (a) and (b) in Figs. 3-5. It should be noted, however, that experimental reports of nanoparticle haloing [48–52] have been mostly confined to mixtures of oppositely-charged colloids and nanoparticles.

For the macroion valences considered here, the trends in colloidal structure are accurately captured by the one-component model. With increasing valences, however, qualitative deviations emerge, reflecting limitations of our approximations. Within

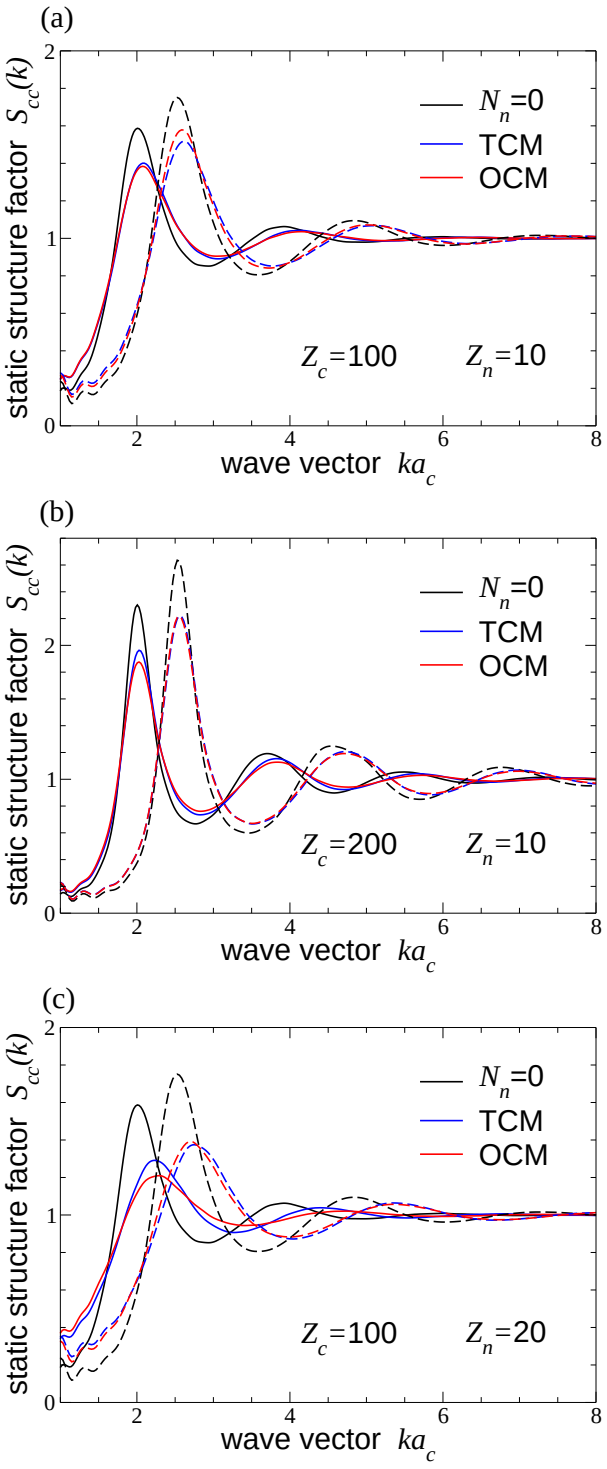

FIG. 6. Colloid-colloid static structure factors corresponding to radial distribution functions in Figs. 3-5. Blue, red, and black curves are, respectively, $S_{cc}(k)$ in the two-component model (TCM), scaled according to Eq. (65) for direct comparison, the one-component model (OCM), and the nanoparticle-free suspension ($N_n = 0$). Colloid volume fractions are $\phi_c = 0.1$ (solid curves) and 0.2 (dashed curves). Beyond main peak, TCM and OCM curves are barely distinguishable.

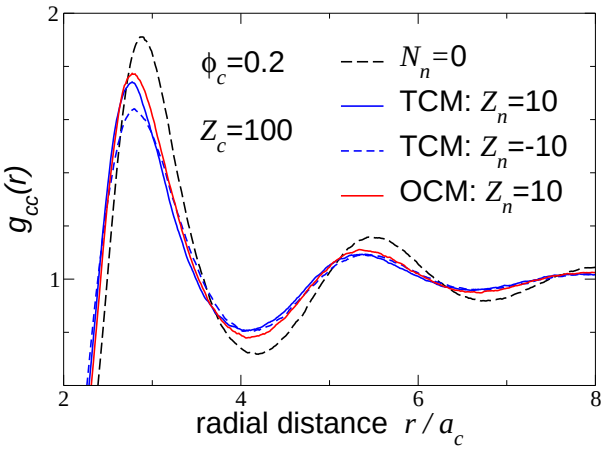

FIG. 7. Colloid-colloid radial distribution function for same parameters as in Fig. 3(b), except that, in the two-component model (TCM), nanoparticle valence is either $Z_n = 10$ or $Z_n = -10$. In the one-component model (OCM), $v_{\rm eff}(r)$, and thus $g_{cc}(r)$, are independent of the sign of Z_n.

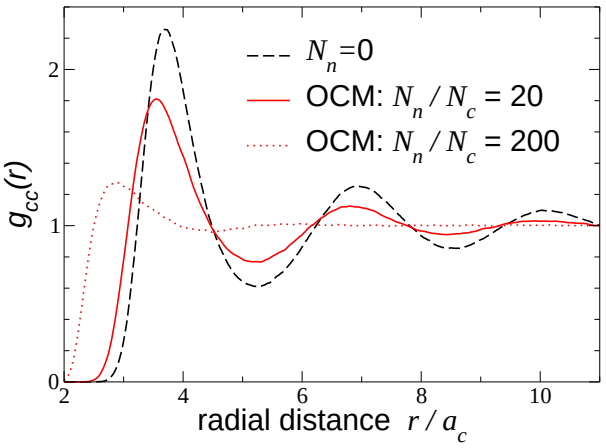

FIG. 8. Colloid-colloid radial distribution functions from simulations of the one-component model (OCM) for system parameters comparable to experiments of ref. [52]: $a_c = 285$ nm, $a_n = 2.57$ nm, $Z_c = 350$, $Z_n = 10$, and $\phi_c = 0.1$. The nanoparticle-to-colloid ratio varies from 0 (dashed black) to 20 (solid red) to 200 (dotted red).

the primitive model of charged colloids, the linear-response approximation, from which the Yukawa effective pair potentials [Eqs. (5)-(7)] are derived, proves accurate, compared with simulations and Poisson-Boltzmann theory [45–47], when the potential energy of a counterion at one diameter from the macroion center is less than $\sim 3\ k_BT$ in magnitude. This condition is equivalent to the criterion $|Z_c|\lambda_B/a_c \lesssim 6$. (Beyond this threshold, where nonlinear counterion response becomes significant, charge renormalization schemes extend the linear-response regime by incorporating nonlinear effects

into effective interaction parameters [45–47].) By extension, a similar condition should constrain the validity of the linear-response approximation applied to colloid-nanoparticle mixtures [Eq. (16)]. Thus, we postulate that the potential energy of a charged nanoparticle at one colloid diameter from the center of a colloidal macroion should not exceed $\sim 3\ k_BT$ in magnitude. This condition is roughly equivalent to the criterion:

$$\Gamma_n \equiv \frac{\lambda_B |Z_c Z_n|\ e^{-\kappa(a_c - a_n)}}{a_c(1+\kappa a_c)(1+\kappa a_n)} \lesssim 6\ . \qquad (66)$$

Based on this guiding criterion, the systems represented in Figs. 3-5 lie within the linear-response regime, while systems with significantly larger valences (e.g., $Z_c = 200$ and $Z_n = 20$) do not. It should be noted that, while we have selected system parameters that probe the limits of Eq. (66), most experimental systems fall within the linear regime.

The simulation data reported above are limited to like-charged mixtures. As noted in Sec. III, the effective pair potential in the OCM is invariant under a change of signs of the macroion charges. This predicted symmetry is tested in Fig. 7, which plots $g_{cc}(r)$ from simulations for $Z_c = 100$ and $Z_n = \pm 10$. For these relatively low valences, differences between the $Z_n = 10$ and $Z_n = -10$ curves are minor, in reasonable agreement with the OCM prediction. With increasing valence, however, the differences in structure between like- and oppositely-charged mixtures become more significant and deviations between the TCM and OCM rapidly grow. This symmetry breaking is caused by failure of the linear-response approximation when highly charged nanoparticles are strongly attracted to and accumulate around oppositely-charged colloids. Incorporating adsorbed or closely associated nanoparticles into the effective, renormalized charge of the colloids, however, can considerably extend the linear-response regime [45–47].

B. Comparison with Experiments

Finally, to demonstrate a practical application of the effective interaction theory, we turn to the experiments of ref. [52], which investigated mixtures of weakly-charged silica microspheres and strongly charged hydrous zirconia nanoparticles dispersed in deionized water. Although this system exhibits van der Waals attraction between colloids and nanoparticles, adsorbed nanoparticles may be viewed as contributing to the effective colloidal charge. Thus, we include in our model only electrostatic interactions to isolate the influence on structure and stability of screening by free (nonadsorbed) nanoparticles.

For comparison with the experiments, we set the colloid and nanoparticle radii to the measured values of $a_c = 285$ nm and $a_n = 2.57$ nm. For the macroion valences, we set $Z_c = 350$ (weakly-charged colloids) and $Z_n = 10$ (relatively strongly charged nanoparticles), consistent with the estimated zeta potentials of $\zeta_c \sim 1$ mV and $\zeta_n \sim 70$ mV. From the reported colloid and nanoparticle volume fractions, $\phi_c = 0.1$ and $\phi_n = 0.00185$, nanoparticles outnumbered colloids by a factor $N_n/N_c = O(10^4)$. At such high concentrations, the Debye screening length, $\kappa^{-1} \sim O(10)$ nm, is so short that electrostatic interactions are virtually entirely screened. To explore the effect of longer screening lengths, we varied the nanoparticle-to-colloid ratio in the range from 0 to 200.

While simulations of the two-component model with $O(10^5)$ explicit nanoparticles – let alone the primitive model with $O(10^6)$ explicit microions – would be computationally expensive, a simulation of $O(10^3)$ colloids in the OCM takes only a few hours on a desktop computer. Figure 8 shows our results for the colloid-colloid radial distribution functions. In the absence of free nanoparticles, the suspension is in a relatively structured, charge-stabilized, fluid state. With increasing nanoparticle concentration, however, the growing screening effect of the nanoparticles progressively weakens correlations between colloids, consistent with destabilization of the suspension observed in the experiments.

VI. CONCLUSIONS

In summary, we have developed a theory of effective interactions, based on a sequential coarse-graining scheme, that maps a mixture of charged colloids and nanoparticles first onto a two-component mixture of pseudo-macroions and then onto a one-component model of only pseudo-colloids governed by effective interactions. In linear-response and mean-field approximations for the nanoparticle response to the colloid-nanoparticle interaction, the effective pair potential has the same Yukawa form as in the coarse-grained mixture model, but with modified screening constant and amplitude that depend nontrivially on nanoparticle properties. Nanoparticles enhance the screening of electrostatic interactions between colloids to an extent that increases with nanoparticle size, charge, and concentration.

By performing molecular dynamics simulations of the two-component and one-component models, we computed structural properties and validated the theory for systems with moderate electrostatic coupling strengths, where the linear-response and mean-field approximations are justified. For system parameters consistent with recent experimental stud-

ies of mixtures of silica microspheres and zirconia nanoparticles, we showed that charged nanoparticles can substantially weaken correlations between charged colloids, promoting phase instability at sufficiently high nanoparticle concentrations, qualitatively consistent with observations.

The theory developed here has the potential to vastly reduce the computational effort needed to model multicomponent mixtures. When applied within the linear-response regime, the theory can guide experiments and simulations of more explicit models by facilitating surveys of multidimensional parameter spaces that are typical of nanocomposite soft materials. The theory also offers conceptual insights into how specific nanoparticle properties influence electrostatic screening.

As an outlook for future work, the theory can predict, beyond structural properties, also thermodynamic properties of colloid-nanoparticle mixtures. Phase diagrams can be computed from the total free energy (including the volume energy), which can be approximated using variational perturbation theory [30, 32], or from the osmotic pressure, which can be computed from the virial theorem for density-dependent effective interactions [32, 47]. For this purpose, the practical range of the theory could be extended beyond the linear-response regime by developing a charge renormalization scheme analogous to that established for charged colloids [45–47]. The sequential coarse-graining scheme also can be extended to more complex mixtures with distributions of macroion size, valence, and concentration. Furthermore, the same approach could be adapted to other macroion architectures, e.g., polyelectrolyte microgels, microcapsules, and vesicles, which may be permeable or semipermeable to nanoparticles.

ACKNOWLEDGMENTS

This work was supported by the National Science Foundation under Grant No. DMR-1106331. Helpful discussions with Jun Kyung Chung and Braden Weight are gratefully acknowledged.

Appendix A: Explicit Evaluation of Integrals

For completeness, we outline the explicit evaluation of real-space convolution integrals that appear in Sec. III. We begin with the integral in Eq. (36):

$$I_1(r) = \int_{-1}^{1} d\mu \int_0^\infty dr'\, r' e^{-qr'} f(|\mathbf{r}-\mathbf{r}'|) \ ,$$

where

$$f(r) = \begin{cases} \dfrac{e^{-\kappa r}}{r} \ , & r \geq a_{cn} \\ \alpha\, \dfrac{e^{-\kappa_0}}{a_{cn}} \ , & r < a_{cn} \ . \end{cases}$$

and $\mu \equiv \cos\theta$, θ being the angle between position vectors $\mathbf{r}$ and $\mathbf{r}'$. Since $f(r)$ is a Yukawa function outside a sphere of radius a_{cn} and a constant inside, we split $I_1(r)$ into three relatively tractable integrals:

$$I_1(r) = I_{11}(r) - I_{12}(r) + \alpha \frac{e^{-\kappa_o}}{a_{cn}} I_{13}(r) \ , \tag{A1}$$

where

$$I_{11}(r) = \int_0^\infty ds\, s e^{-qs}\, I_\mu(\kappa, r, s) \ , \tag{A2}$$

$$I_{12}(r) = \int_0^{a_{cn}} ds\, s e^{-\kappa s}\, I_\mu(q, r, s) \ , \tag{A3}$$

$$I_{13}(r) = \int_0^{a_{cn}} ds\, s^2\, I_\mu(q, r, s) \ , \tag{A4}$$

with

$$I_\mu(\gamma, r, s) \equiv \int_{-1}^{1} d\mu\, \frac{e^{-\gamma|\mathbf{r}-\mathbf{s}|}}{|\mathbf{r}-\mathbf{s}|} \ . \tag{A5}$$

Using the substitutions $t = \sqrt{r^2+s^2}$, $u = 2rs/t^2$, and $x = \sqrt{1-u\mu}$, we can write

$$\begin{aligned} I_\mu(\gamma, r, s) &= \frac{1}{t} \int_{-1}^{1} d\mu\, \frac{e^{-\gamma t\sqrt{1-u\mu}}}{\sqrt{1-u\mu}} \\ &= \frac{t}{rs} \int_{|r-s|/t}^{(r+s)/t} dx\, e^{-\gamma t x} \\ &= \frac{e^{-\gamma|r-s|} - e^{-\gamma(r+s)}}{\gamma rs} \ . \end{aligned} \tag{A6}$$

Substituting Eq. (A6) into Eq. (A2), we have

$$\begin{aligned} I_{11}(r) &= \frac{1}{\kappa r} \int_0^\infty ds\, s e^{-qs} \left(e^{-\kappa|r-s|} - e^{-\kappa(r+s)} \right) \\ &= \frac{2}{\kappa_n^2 r} \left(e^{-\kappa r} - e^{-qr} \right) \ . \end{aligned} \tag{A7}$$

Next, substituting Eq. (A6) into Eq. (A3) yields

$$I_{12}(r) = \frac{1}{qr} \int_0^{a_{cn}} ds\, e^{-\kappa s} \left(e^{-q|r-s|} - e^{-q(r+s)} \right) \ , \tag{A8}$$

which gives for $r \geq a_{cn}$,

$$I_{12}(r) = \frac{1}{qr}\int_0^{a_{cn}} ds\, e^{-\kappa s}\,\left(e^{-q(r-s)} - e^{-q(r+s)}\right)$$
$$= \left(\frac{e^{q_0-\kappa_0}}{q-\kappa} + \frac{e^{-\kappa_0-q_0}}{\kappa+q} - \frac{2q}{\kappa_n^2}\right)\frac{e^{-qr}}{qr}\ , \quad \text{(A9)}$$

and for $r < a_{cn}$,

$$I_{12}(r) = \frac{1}{qr}\left[\int_0^{r} ds\, e^{-\kappa s}\,\left(e^{-q(r-s)} - e^{-q(r+s)}\right)\right.$$
$$\left. + \int_r^{a_{cn}} ds\, e^{-\kappa s}\,\left(e^{q(r-s)} - e^{-q(r+s)}\right)\right]$$
$$= \frac{2}{\kappa_n^2 r}\left(e^{-\kappa r} - e^{-qr}\right) - 2\frac{e^{-\kappa_0-q_0}}{\kappa+q}\,\frac{\sinh(qr)}{qr}\ . \quad \text{(A10)}$$

Substituting Eq. (A6) into Eq. (A4) yields

$$I_{13}(r) = \frac{1}{qr}\int_0^{a_{cn}} ds\, s\left(e^{-q|r-s|} - e^{-q(r+s)}\right)\ , \quad \text{(A11)}$$

which gives for $r \geq a_{cn}$,

$$I_{13}(r) = \frac{1}{qr}\int_0^{a_{cn}} ds\, s\left(e^{-q(r-s)} - e^{-q(r+s)}\right)$$
$$= \left[(q_0-1)e^{q_0} + (1+q_0)e^{-q_0}\right]\frac{e^{-qr}}{q^3 r}\ , \quad \text{(A12)}$$

and for $r < a_{cn}$,

$$I_{13}(r) = \frac{1}{qr}\left[\int_0^{r} ds\, s e^{-q(r-s)} + \int_r^{a_{cn}} ds\, s e^{q(r-s)}\right.$$
$$\left. - \int_0^{a_{cn}} ds\, s e^{-q(r+s)}\right]$$
$$= \frac{2}{q^2}\left[1 - (1+q_0)e^{-q_0}\frac{\sinh(qr)}{qr}\right]\ . \quad \text{(A13)}$$

Substituting Eqs. (A7)-(A13) into Eq. (A1), we obtain Eq. (37) and, with α given by Eq. (40),

$$I_1(r) = \begin{cases} \dfrac{2a_{cn}e^{-\kappa_0}}{(1+q_0)(\kappa_0+q_0)}\ , & r < a_{cn}\ , \\ \dfrac{2}{\kappa_n^2 r}\left(e^{-\kappa r} - \dfrac{1+\kappa_0}{1+q_0}e^{-qr+q_0-\kappa_0}\right)\ , & r \geq a_{cn}\ . \end{cases} \quad \text{(A14)}$$

Next, we evaluate the integrals $I_2(r)$ and $I_3(r)$ [Eqs. (50) and (51)] in the range $r \geq 2a_{cn}$, where the effective pair potential in the one-component model is defined. We note first that

$$I_2(r) = \int_0^{a_{cn}} dr'\, r'^2\, I_\mu(\kappa, r, r')\ , \quad \text{(A15)}$$

where $I_\mu(\kappa, r, r')$ is defined in Eq. (A5). Substituting for $I_\mu(\kappa, r, r')$ from Eq. (A6), we have

$$I_2(r) = \frac{1}{\kappa r}\int_0^{a_{cn}} dr'\, r'\left(e^{-\kappa(r-r')} - e^{-\kappa(r+r')}\right)$$
$$= \frac{1}{\kappa^3}\left[(1+\kappa_0)e^{-\kappa_0} - (1-\kappa_0)e^{\kappa_0}\right]\frac{e^{-\kappa r}}{r}\ . \quad \text{(A16)}$$

The integral $I_3(r)$ can be split into two pieces:

$$I_3(r) = I_1(r) - I'_{12}(r)\ , \quad \text{(A17)}$$

where $I_1(r)$ is the same integral as in Eq. (36) and $I'_{12}(r)$ is the same as $I_{12}(r)$ in Eqs. (A3) and (A9), except with κ and q interchanged:

$$I'_{12}(r) = \int_0^{a_{cn}} ds\, s e^{-qs}\, I_\mu(\kappa, r, s)$$
$$= \left(\frac{e^{\kappa_0-q_0}}{\kappa-q} + \frac{e^{-\kappa_0-q_0}}{\kappa+q} + \frac{2\kappa}{\kappa_n^2}\right)\frac{e^{-\kappa r}}{\kappa r}\ . \quad \text{(A18)}$$

Thus, we finally obtain

$$I_3(r) = -\frac{2}{\kappa_n^2}e^{q_0-\kappa_0}\,\frac{1+\kappa_0}{1+q_0}\,\frac{e^{-qr}}{r}$$
$$- \left(\frac{e^{\kappa_0-q_0}}{\kappa-q} + \frac{e^{-\kappa_0-q_0}}{\kappa+q}\right)\frac{e^{-\kappa r}}{\kappa r}\ . \quad \text{(A19)}$$

[1] P.-G. de Gennes and J. Badoz, *Fragile Objects* (Springer-Verlag, New York, 1996).
[2] R. A. L. Jones, *Soft Condensed Matter* (Oxford, Oxford, 2002).
[3] J. Israelachvili, *Intermolecular and Surface Forces* (Academic, London, 1992).
[4] P. N. Pusey, "Colloidal suspensions," in *Liquids, Freezing and Glass Transition, Les Houches session 51*, Vol. 2, edited by J.-P. Hansen, D. Levesque, and J. Zinn-Justin (North-Holland, Amsterdam, 1991) pp. 763–931.
[5] D. F. Evans and H. Wennerström, *The Colloidal Domain*, 2nd ed. (Wiley-VCH, New York, 1999).
[6] C. N. Likos, Phys. Rep. **348**, 267 (2001).
[7] A. R. Denton, in *Nanostructured Soft Matter: Experiment, Theory, Simulation and Perspectives*, edited by A. V. Zvelindovsky (Springer, 2007) pp. 395–433.
[8] G. N. Patey, J. Chem. Phys. **72**, 5763 (1980).
[9] L. Belloni, Phys. Rev. Lett. **57**, 2026 (1986).
[10] S. Khan and D. Ronis, Mol. Phys. **60**, 637 (1987).
[11] S. Khan, T. L. Morton, and D. Ronis, Phys. Rev. A **35**, 4295 (1987).
[12] M. D. Carbajal-Tinoco and P. González-Mozuelos, J. Chem. Phys. **117**, 2344 (2002).
[13] S. N. Petris and D. Y. C. Chan, J. Chem. Phys. **116**, 8588 (2002).
[14] J. A. Anta and S. Lago, J. Chem. Phys. **116**, 10514 (2002).
[15] V. Morales, J. A. Anta, and S. Lago, Langmuir **19**, 475 (2003).
[16] L. B. Bhuiyan and C. W. Outhwaite, J. Chem. Phys. **116**, 2650 (2002).
[17] P. B. Warren, J. Chem. Phys. **112**, 4683 (2000).
[18] P. B. Warren, J. Phys.: Condens. Matter **15**, S3467 (2003).
[19] P. B. Warren, Phys. Rev. E **73**, 011411 (2006).
[20] B. Beresford-Smith, D. Y. C. Chan, and D. J. Mitchell, J. Coll. Int. Sci. **105**, 216 (1985).
[21] D. Y. C. Chan, Phys. Rev. E **63**, 061806 (2001).
[22] D. Y. C. Chan, P. Linse, and S. N. Petris, Langmuir **17**, 4202 (2001).
[23] R. van Roij and J. P. Hansen, Phys. Rev. Lett. **79**, 3082 (1997).
[24] R. van Roij, M. Dijkstra, and J.-P. Hansen, Phys. Rev. E **59**, 2010 (1999).
[25] R. van Roij and R. Evans, J. Phys.: Condens. Matter **11**, 10047 (1999).
[26] H. Graf and H. Löwen, Phys. Rev. E **57**, 5744 (1998).
[27] M. J. Grimson and M. Silbert, Mol. Phys. **74**, 397 (1991).
[28] A. R. Denton, in *in Electrostatics of Soft and Disordered Matter*, edited by D. S. Dean, J. Dobnikar, A. Naji, and R. Podgornik (Pan Stanford, Singapore, 2014) pp. 201–215.
[29] A. R. Denton, J. Phys.: Condens. Matter **11**, 10061 (1999).
[30] A. R. Denton, Phys. Rev. E **62**, 3855 (2000).
[31] A. R. Denton, Phys. Rev. E **70**, 031404 (2004).
[32] A. R. Denton, Phys. Rev. E **73**, 041407 (2006).
[33] A. R. Denton, Phys. Rev. E **76**, 051401 (2007).
[34] D. Goulding and J.-P. Hansen, Europhys. Lett. **46**, 407 (1999).
[35] J.-P. Hansen, D. Goulding, and R. van Roij, J. Phys. IV **10**, 5 (2000).
[36] S. Alexander, P. M. Chaikin, P. Grant, G. J. Morales, and P. Pincus, J. Chem. Phys. **80**, 5776 (1984).
[37] Y. Levin, E. Trizac, and L. Bocquet, J. Phys.: Condens. Matter **15**, S3523 (2003).
[38] E. Trizac and Y. Levin, Phys. Rev. E **69**, 031403 (2004).
[39] S. Pianegonda, E. Trizac, and Y. Levin, J. Chem. Phys. **126**, 014702 (2007).
[40] R. Castañeda-Priego, L. F. Rojas-Ochoa, V. Lobaskin, and J. C. Mixteco-Sánchez, Phys. Rev. E **74**, 051408 (2006).
[41] L. F. Rojas-Ochoa, R. Castañeda-Priego, V. Lobaskin, A. Stradner, F. Scheffold, and P. Schurtenberger, Phys. Rev. Lett. **100**, 178304 (2008).
[42] T. E. Colla, Y. Levin, and E. Trizac, J. Chem. Phys. **131**, 074115 (2009).
[43] B. Zoetekouw and R. van Roij, Phys. Rev. Lett. **97**, 258302 (2006).
[44] B. Zoetekouw and R. van Roij, Phys. Rev. E **73**, 21403 (2006).
[45] A. R. Denton, J. Phys.: Condens. Matter **20**, 494230 (2008).
[46] B. Lu and A. R. Denton, Commun. Comp. Phys. **7**, 235 (2010).
[47] A. R. Denton, J. Phys.: Condens. Matter **22**, 364108 (2010).
[48] V. Tohver, J. E. Smay, A. Braem, P. V. Braun, and J. A. Lewis, PNAS **98**, 8950 (2001).
[49] V. Tohver, A. Chan, O. Sakurada, and J. A. Lewis, Langmuir **17**, 8414 (2001).
[50] A. T. Chan and J. A. Lewis, Langmuir **21**, 8576 (2005).
[51] A. T. Chan and J. A. Lewis, Langmuir **24**, 11399 (2008).
[52] F. Zhang, G. G. Long, P. R. Jemian, J. Ilavsky, V. T. Milam, and J. A. Lewis, Langmuir **24**, 6504 (2008).
[53] C. J. Martinez, J. Liu, S. K. Rhodes, E. Luijten, E. R. Weeks, and J. A. Lewis, Langmuir **21**, 9978 (2005).
[54] J. F. Gilchrist, A. T. Chan, E. R. Weeks, and J. A. Lewis, Langmuir **21**, 11040 (2005).
[55] X. Hong and G. A. Willing, Langmuir **25**, 4929 (2009).
[56] S. Buzzaccaro, R. Piazza, J. Colombo, and A. Parola, J. Chem. Phys. **132**, 124902 (2010).
[57] S. Savarala, S. Ahmed, M. A. Ilies, and S. L. Wunder, ACS Nano **5**, 2619 (2011).
[58] X. Xing, G. Sun, Z. Li, and T. Ngai, Langmuir **28**, 16022 (2012).

[59] D. Herman and J. Y. Walz, Langmuir **29**, 5982 (2013).
[60] D. Herman and J. Y. Walz, Langmuir **31**, 4844 (2015).
[61] S. N. Kazi, A. Badarudin, M. N. M. Zubir, H. N. Ming, M. Misran, E. Sadeghinezhad, M. Mehrali, and N. I. Syuhada, Nanoscale Res. Lett. **10**, 212 (2015).
[62] D. Herman and J. Y. Walz, J. Coll. Interf. Sci. **449**, 143 (2015).
[63] M. N. M. Zubir, A. Badarudin, S. Kazi, M. Misran, A. Amiri, R. Sadri, and S. Khalid, J. Coll. Interf. Sci. **454**, 245 (2015).
[64] R. Krause, B. D'Aguanno, J. M. Méndez-Alcaraz, G. Nägele, R. Klein, and R. Weber, J. Phys.: Condens. Matter **3**, 4459 (1991).
[65] B. D'Aguanno, R. Krause, J. M. Méndez-Alcaraz, and R. Klein, J. Phys.: Condens. Matter **4**, 3077 (1992).
[66] H. Löwen, J.-N. Roux, and J.-P. Hansen, J. Phys.: Condens. Matter **3**, 997 (1991).
[67] H. Ruiz-Estrada, M. Medina-Noyola, and G. Nägele, Physica A **168**, 919 (1990).
[68] B. D'Aguanno and R. Klein, Phys. Rev. A **46**, 7652 (1992).
[69] S. Karanikas and A. A. Louis, Phys. Rev. Lett. **93**, 248303 (2004).
[70] M. Chávez-Páez, P. González-Mozuelos, M. Medina-Noyola, and J. Méndez-Alcaraz, Physica A **341**, 1 (2004).
[71] E. N. Scheer and K. S. Schweizer, J. Chem. Phys. **128**, 164905 (2008).
[72] L. E. Sánchez-Díaz, A. Vizcarra-Rendón, and M. Medina-Noyola, J. Chem. Phys. **132**, 234506 (2010).
[73] L. E. Sánchez-Díaz, G. A. Mendez-Maldonado, M. González-Melchor, H. Ruiz-Estrada, and M. Medina-Noyola, J. Chem. Phys. **135**, 14504 (2011).
[74] A. Torres, A. Cuetos, M. Dijkstra, and R. van Roij, Phys. Rev. E **77**, 031402 (2008).
[75] A. Torres, G. Téllez, and R. van Roij, J. Chem. Phys. **128**, 154906 (2008).
[76] J. M. Falcón-González and R. Castañeda-Priego, Phys. Rev. E **83**, 041401 (2011).
[77] H. Huang and E. Ruckenstein, J. Phys. Chem. B **117**, 6318 (2013).
[78] H. Huang and E. Ruckenstein, Colloid Surface A **436**, 862 (2013).
[79] A. A. Louis, E. Allahyarov, H. Löwen, and R. Roth, Phys. Rev. E **65**, 061407 (2002).
[80] J. Liu and E. Luijten, Phys. Rev. Lett. **93**, 247802 (2004).
[81] J. Rydén, M. Ullner, and P. Linse, J. Chem. Phys. **123**, 034909 (2005).
[82] E. Sanz, C. Valeriani, D. Frenkel, and M. Dijkstra, Phys. Rev. Lett. **99**, 055501 (2007).
[83] M. Bier, R. van Roij, and M. Dijkstra, J. Chem. Phys. **133**, 124501 (2010).
[84] K. Barros and E. Luijten, Phys. Rev. Lett. **113**, 017801 (2014).
[85] J. K. Chung and A. R. Denton, Phys. Rev. E **88**, 022306 (2013).
[86] J. P. Hansen and I. R. McDonald, *Theory of Simple Liquids* (London, 1986).
[87] A. P. dos Santos, A. Bakhshandeh, A. Diehl, and Y. Levin, Soft Matter **12**, 8528 (2016).
[88] P. González-Mozuelos and M. D. Carbajal-Tinoco, J. Chem. Phys. **109**, 11074 (1998).
[89] R. Castañeda-Priego, A. Rodríguez-López, and J. M. Méndez-Alcaraz, Phys. Rev. E **73**, 051404 (2006).
[90] D. Léger and D. Levesque, J. Chem. Phys. **123**, 124910 (2005).
[91] M. Heinen, T. Palberg, and H. Löwen, J. Chem. Phys. **140**, 124904 (2014).
[92] M. Heinen, E. Allahyarov, and H. Löwen, J. Comput. Chem. **35**, 275 (2014).
[93] P. González-Mozuelos, M. Medina-Noyola, B. D'Aguanno, J. M. Méndez-Alcaraz, and R. Klein, J. Chem. Phys. **95**, 2006 (1991).
[94] P. González-Mozuelos, J. Alejandre, and M. Medina-Noyola, J. Chem. Phys. **97**, 8712 (1992).
[95] `http://lammps.sandia.gov`.
[96] S. Plimpton, J. Comp. Phys. **117**, 1 (1995).
[97] B. M. Weight and A. R. Denton, unpublished.